Electronic correlations of small diameter carbon nanotubes

2006 J. Phys.: Condens. Matter 18 S2105

(http://iopscience.iop.org/0953-8984/18/33/S26)

INSTITUTE OF PHYSICS PUBLISHING JOURNAL OF PHYSICS: CONDENSED MATTER

J. Phys.: Condens. Matter **18** (2006) S2105–S2114 doi:10.1088/0953-8984/18/33/S26

Electronic correlations of small diameter carbon nanotubes

E Perfetto[1,2] **and J González**[1]

[1] Instituto de Estructura de la Materia, Consejo Superior de Investigaciones Científicas, Serrano 123, 28006 Madrid, Spain
[2] Istituto Nazionale di Fisica Nucleare, Laboratori Nazionali di Frascati, Via E Fermi 40, 00044 Frascati, Italy

Received 10 January 2006, in final form 31 January 2006
Published 4 August 2006
Online at stacks.iop.org/JPhysCM/18/S2105

Abstract

The transport properties of 4 Å diameter carbon nanotubes have been studied in recent experiments by Tang *et al*, and evidence of superconductivity at about 15 K has been claimed. The only metallic nanotubes compatible with such a small radius are the (3, 3) armchair and the (5, 0) zigzag respectively. In this paper we study the electronic properties of both these systems, paying special attention to the screening effects coming from the surrounding environment characterizing the experimental set-up. We look for the low temperature instabilities in the Luttinger liquid description of the correlated electron system. The phase diagram is investigated by taking into account the competition between the Coulomb repulsion and the phonon-mediated electron–electron interaction.

1. Introduction

Carbon nanotubes are wrapped graphene sheets with a cylindrical shape. Typical nanotubes have radii of the order of 1–10 nm and lengths of some microns. There are some special conditions where it is possible to synthesize much smaller samples, with a diameter of only 0.4 nm [1]. This can be realized by growing carbon nanotubes within the narrow channels of a zeolite matrix. Such a technique provides large 3D arrays of isolated and well aligned tubes, whose only possible geometries are the zigzag (5, 0) and the (3, 3) armchair respectively. The most interesting feature of these ultrasmall nanotubes consists in the observation of superconductivity at 15 K claimed by Tang and collaborators [2]. In this experiment a strong diamagnetic behaviour at low temperature was interpreted as a Meissner effect, but a genuine superconducting transition, signalled by a drop of the resistance, was not observed.

In this paper we wish to investigate the low energy properties of both (5, 0) and (3, 3) nanotubes, paying special attention to the influence of the surrounding environment. We use the bosonization technique to study the Luttinger liquid behaviour of the system, which is the normal phase of one-dimensional interacting electrons; then we apply the renormalization

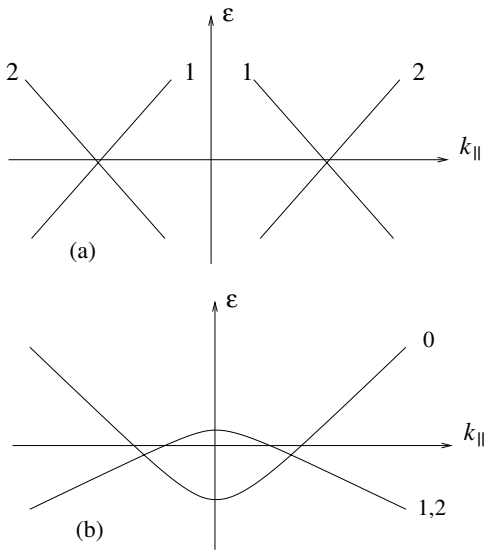

Figure 1. Low energy band structure of (3, 3) nanotubes (a), and (5, 0) nanotubes (b). $k_\parallel$ denotes the longitudinal momentum.

group approach to analyse the low energy instabilities of the electronic ground state [3]. We find that in the (5, 0) geometry weak superconducting correlations develop, but the low energy phase is indeed characterized by divergence of the compressibility in the charge sector. In the (3, 3) geometry there is no signal of superconductivity, but a divergence of the diamagnetic susceptibility is observed, in qualitative agreement with the experimental finding of [2].

2. Band structure and the catalogue of the interactions

In this section we describe the band structure of (3, 3) and (5, 0) nanotubes. On the basis of this, we build a complete catalogue of interactions between electrons on the Fermi surface.

The (3, 3) nanotube shows the typical band structure of armchair tubes. There are two subbands (labelled 1, 2) crossing the Fermi level, giving rise to four linear branches around the two Fermi momenta $\pm k_F = \pm 2\pi/3a$, where $a = 2.46$ Å is the graphite lattice constant (see figure 1(a)). The interaction processes among electrons at the Fermi level can be classified by attaching to them respective coupling constants $g_i^{(j)}$ [4]. The lower index indicates whether the interacting particles shift from one Fermi point to the other ($i = 1$), remain at different Fermi points ($i = 2$) or interact near the same Fermi point ($i = 4$). The upper label follows the same rule for classifying different combinations of left- and right-movers, including the possibility of having Umklapp processes ($j = 3$) in the undoped system. The catalogue is completed by introducing *intertube* couplings $\tilde{g}_i^{(j)}$ which follow the convention described above, but involve electronic currents located at nearest neighbour nanotubes. The latter processes are due to the long range nature of the Coulomb interaction and must be included in order to properly model the experimental samples studied in [2].

The (5, 0) nanotubes have a different band structure since there are three subbands crossing the Fermi level (in the undoped system) [5, 6]. The position of the different Fermi points in momentum space is shown in figure 1(b). They correspond to two degenerate subbands with opposite values of the angular momentum around the nanotube axis (denoted by 1, 2) and a

third subband with zero angular momentum (labelled by 0 in the figure). The Fermi velocities are different in the nondegenerate and degenerate subbands, being smaller in either case than for nanotubes of normal radius and leading to an enhanced density of states at low energies. As regards the catalogue of interactions, we first borrow the classification that has been already made for (3, 3) nanotubes for electrons in subbands 1 and 2. Anyway, the above set of couplings $g_i^{(j)}$ has to be supplemented with couplings for the channels involving processes between a particle at one of the degenerate subbands 1, 2 and another at the nondegenerate subband 0. Now we can distinguish between interactions that keep each particle within its respective subband, to which we assign a coupling $f^{(2)}$ ($f^{(4)}$) for particles of opposite (like) chirality, and backscattering interactions that lead to the exchange of the subbands for the two particles ($f^{(1)}$). Moreover, we have also channels in which the particles interact within the outer subband, and that we will label as in the usual g-ology description, in terms of the couplings $g^{(1)}$, $g^{(2)}$ and $g^{(4)}$. Finally, there are also interaction processes in which two particles with about zero total momentum exchange their position from the outer to the inner subbands, or vice versa. We will assign the coupling u_{F} to that kind of interaction with no change of chirality of the particles, and the coupling u_{B} when there is a change in their chirality. As in the (3, 3) case, the intertube couplings follow the same notation, but carry the tilde label.

The strength of each process depends on the competition between the Coulomb repulsion and the phonon-mediated electron–electron interaction. The Coulomb potential in the wrapped geometry reads [7]

$$V_{\mathrm{C}}(\mathbf{r}-\mathbf{r}') = \frac{e^2/\kappa}{\sqrt{(x-x')^2 + 4R^2\sin^2[(y-y')^2/2R^2] + a_z^2}} \tag{1}$$

where $a_z \simeq 1.6$ Å, R is the nanotube radius and κ is the dielectric constant depending on the environment hosting the nanotubes. The Coulomb contribution to the coupling constants is obtained by Fourier transforming the electrostatic potential $V_{\mathrm{C}}(\mathbf{r}-\mathbf{r}')$ by using the appropriate momentum transfer q corresponding to each process [8].

We point out that for small values of q, i.e. forward scattering processes, the Coulomb contribution is strongly affected by the screening effects due to the surrounding 3D array of nanotubes in the zeolite matrix. Therefore we calculate such a contribution by using a generalized RPA scheme [9], where the interaction among all the nanotubes is taken into account. It is found that for distances much larger than the nanotube separation, the array effectively screens the Coulomb interaction, as a 3D system, rendering the Coulomb potential within each nanotube short ranged.

The phonon-mediated contribution for the intertube processes is obtained by borrowing from the literature the strength of the electron–phonon couplings and the frequencies of the normal modes relevant at the Fermi level [10–12].

3. Renormalization group analysis

In carbon nanotubes, the 1D nature of the electron modes close to the Fermi energy makes it possible to solve exactly the system with just the forward scattering interactions $g_{2,4}^{(2,4)}$ (plus $g^{(2,4)}$ and $f^{(2,4)}$ for the (5, 0) case). This can be realized by means of bosonization techniques, where the interacting electron Hamiltonian becomes that of a set of noninteracting boson fields [3]. This picture is what characterizes the Luttinger liquid regime of the electron system. Within this scheme, the forward coupling constants dictate thermodynamic and transport properties such as the compressibility, the Drude weight and the specific heat, through algebraic functions of the renormalized velocities u_i and the so-called Luttinger liquid parameters K_i.

For instance, in the (3, 3) case it holds that

$$u_\pm K_\pm = v_\mathrm{F} + (1/\pi)\left(g_4^{(4)} \pm g_2^{(4)} - (g_2^{(2)} \pm g_4^{(2)})\right) \tag{2}$$

$$u_\pm / K_\pm = v_\mathrm{F} + (1/\pi)\left(g_4^{(4)} \pm g_2^{(4)} + (g_2^{(2)} \pm g_4^{(2)})\right), \tag{3}$$

and therefore

$$\kappa_\pm = \frac{2}{\pi}\frac{K_\pm}{u_\pm} \tag{4}$$

$$D_\pm = 2u_\pm K_\pm \tag{5}$$

$$\frac{C_v}{T} = \frac{\pi}{3}\left(\frac{1}{u_+} + \frac{1}{u_-}\right), \tag{6}$$

where $\kappa_\pm$ are the compressibilities, $D_\pm$ the Drude weights and C_v the specific heat [13].

This picture must be complemented by including the backscattering and the Umklapp interactions, which tend to destabilize the Luttinger liquid regime at low temperatures. The relevance of these perturbations comes from the fact that they give rise to quantum corrections that depend logarithmically on the energy scale. By following the renormalization group programme, we can translate the logarithmic dependence on energy of the terms in the diagrammatic expansion into a scale dependence of the renormalized coupling constants [3].

3.1. (3, 3) nanotube

One-loop scaling equations for the $g_i^{(j)}$ couplings have been already written for a model with two subbands in [4]. Here we have completed the set of equations and incorporated a nonperturbative improvement by writing the exact dependence of the anomalous dimensions on the forward scattering couplings through the K_i and by incorporating the corrections coming from the intertube interactions.

The complete set of scaling equations for the (3, 3) nanotube reads

$$\frac{\partial g_1^{(1)}}{\partial l} = -\frac{1}{\pi v_\mathrm{F}}(g_1^{(1)}g_1^{(1)} + g_1^{(2)}g_2^{(1)} + g_1^{(3)}g_1^{(3)} - g_1^{(3)}g_2^{(3)}) \tag{7}$$

$$\frac{\partial g_1^{(2)}}{\partial l} = \left(1 - \frac{1}{K_-}\right)g_1^{(2)} - \frac{1}{\pi v_\mathrm{F}}(g_2^{(1)}g_1^{(1)} - g_4^{(3)}g_1^{(3)}) \tag{8}$$

$$\frac{\partial g_1^{(3)}}{\partial l} = (1 - K_+)g_1^{(3)} - \frac{1}{\pi v_\mathrm{F}}(2g_1^{(3)}g_1^{(1)} - g_2^{(3)}g_1^{(1)} - g_4^{(3)}g_1^{(2)}) \tag{9}$$

$$\begin{aligned}\frac{\partial g_2^{(1)}}{\partial l} = {} & \left(1 - \frac{1}{K_-}\right)g_2^{(1)} - \frac{1}{\pi v_\mathrm{F}}(2g_4^{(1)}g_2^{(1)} - g_4^{(1)}g_1^{(2)} + g_1^{(2)}g_1^{(1)} + g_4^{(3)}g_2^{(3)} \\ & - g_4^{(3)}g_1^{(3)} + 12\tilde{g}_4^{(1)}\tilde{g}_2^{(1)} + 12\tilde{g}_4^{(3)}\tilde{g}_2^{(3)})\end{aligned} \tag{10}$$

$$\frac{\partial g_2^{(2)}}{\partial l} = -\frac{1}{2\pi v_\mathrm{F}}(g_2^{(1)}g_2^{(1)} + g_1^{(1)}g_1^{(1)} + g_1^{(2)}g_1^{(2)} - g_2^{(3)}g_2^{(3)}) \tag{11}$$

$$\begin{aligned}\frac{\partial g_2^{(3)}}{\partial l} = {} & (1 - K_+)g_2^{(3)} - \frac{1}{\pi v_\mathrm{F}}(2g_4^{(1)}g_2^{(3)} + g_4^{(3)}g_2^{(1)} - g_4^{(3)}g_1^{(2)} - g_4^{(1)}g_1^{(3)} \\ & + 12\tilde{g}_4^{(1)}\tilde{g}_2^{(3)} + 12\tilde{g}_4^{(3)}\tilde{g}_2^{(1)})\end{aligned} \tag{12}$$

$$\begin{aligned}\frac{\partial g_4^{(1)}}{\partial l} = {} & -\frac{1}{\pi v_\mathrm{F}}(g_4^{(1)}g_4^{(1)} + g_2^{(1)}g_2^{(1)} - g_1^{(2)}g_2^{(1)} + g_2^{(3)}g_2^{(3)} - g_2^{(3)}g_1^{(3)} \\ & + 6\tilde{g}_4^{(1)}\tilde{g}_4^{(1)} + 6\tilde{g}_2^{(1)}\tilde{g}_2^{(1)} + 6\tilde{g}_4^{(3)}\tilde{g}_4^{(3)} + 6\tilde{g}_2^{(3)}\tilde{g}_2^{(3)})\end{aligned} \tag{13}$$

$$\frac{\partial g_4^{(2)}}{\partial l} = -\frac{1}{2\pi v_F}(g_4^{(1)}g_4^{(1)} - g_1^{(2)}g_1^{(2)} - g_1^{(3)}g_1^{(3)} - g_4^{(3)}g_4^{(3)}) \tag{14}$$

$$\frac{\partial g_4^{(3)}}{\partial l} = \left(2 - K_+ - \frac{1}{K_-}\right)g_4^{(3)} - \frac{1}{\pi v_F}(g_4^{(3)}g_4^{(1)} + 2g_2^{(3)}g_2^{(1)} - g_1^{(3)}g_2^{(1)} - g_2^{(3)}g_1^{(2)} - g_1^{(3)}g_1^{(2)} + 12\tilde{g}_4^{(1)}\tilde{g}_4^{(3)} + 12\tilde{g}_2^{(1)}\tilde{g}_2^{(3)})$$

$$\frac{\partial \tilde{g}_2^{(1)}}{\partial l} = -\frac{1}{\pi v_F}(2g_4^{(1)}\tilde{g}_2^{(1)} + 2g_2^{(1)}\tilde{g}_4^{(1)} + 4\tilde{g}_4^{(1)}\tilde{g}_2^{(1)} + \tilde{g}_2^{(2)}\tilde{g}_2^{(1)} - g_4^{(2)}\tilde{g}_2^{(1)} - g_1^{(2)}\tilde{g}_4^{(1)} + 2g_2^{(3)}\tilde{g}_4^{(3)} + g_4^{(3)}\tilde{g}_2^{(3)} + 4\tilde{g}_2^{(3)}\tilde{g}_4^{(3)} - g_1^{(3)}\tilde{g}_4^{(3)}) \tag{15}$$

$$\frac{\partial \tilde{g}_2^{(3)}}{\partial l} = -\frac{1}{\pi v_F}(2g_4^{(1)}\tilde{g}_2^{(3)} + 2g_2^{(3)}\tilde{g}_4^{(1)} + 4\tilde{g}_4^{(1)}\tilde{g}_2^{(3)} + g_4^{(3)}\tilde{g}_2^{(1)} + 2g_2^{(1)}\tilde{g}_4^{(3)} + 4\tilde{g}_2^{(1)}\tilde{g}_4^{(3)} - g_1^{(3)}\tilde{g}_4^{(1)} - g_4^{(2)}\tilde{g}_2^{(3)} - g_1^{(2)}\tilde{g}_4^{(3)} - \tilde{g}_2^{(2)}\tilde{g}_2^{(3)}) \tag{16}$$

$$\frac{\partial \tilde{g}_4^{(1)}}{\partial l} = -\frac{1}{\pi v_F}(2g_4^{(1)}\tilde{g}_4^{(1)} + 2g_2^{(1)}\tilde{g}_2^{(1)} + 2\tilde{g}_4^{(1)}\tilde{g}_4^{(1)} + 2\tilde{g}_2^{(1)}\tilde{g}_2^{(1)} + \tilde{g}_4^{(2)}\tilde{g}_4^{(1)} - g_4^{(2)}\tilde{g}_4^{(1)} - g_1^{(2)}\tilde{g}_2^{(1)} + 2g_2^{(3)}\tilde{g}_2^{(3)} + 2\tilde{g}_2^{(3)}\tilde{g}_2^{(3)} + g_4^{(3)}\tilde{g}_4^{(3)} + 2\tilde{g}_4^{(3)}\tilde{g}_4^{(3)} - g_1^{(3)}\tilde{g}_2^{(3)}) \tag{17}$$

$$\frac{\partial \tilde{g}_4^{(3)}}{\partial l} = -\frac{1}{\pi v_F}(2g_4^{(1)}\tilde{g}_4^{(3)} + g_4^{(3)}\tilde{g}_4^{(1)} + 4\tilde{g}_4^{(1)}\tilde{g}_4^{(3)} + 2g_2^{(1)}\tilde{g}_2^{(3)} + 2g_2^{(3)}\tilde{g}_2^{(1)} + 4\tilde{g}_2^{(1)}\tilde{g}_2^{(3)} - g_4^{(2)}\tilde{g}_4^{(3)} - \tilde{g}_4^{(2)}\tilde{g}_4^{(3)} - g_1^{(2)}\tilde{g}_2^{(3)} - g_1^{(3)}\tilde{g}_2^{(1)}) \tag{18}$$

$$\frac{\partial \tilde{g}_4^{(2)}}{\partial l} = -\frac{1}{2\pi v_F}(\tilde{g}_4^{(1)}\tilde{g}_4^{(1)} - \tilde{g}_4^{(3)}\tilde{g}_4^{(3)}) \tag{19}$$

$$\frac{\partial \tilde{g}_2^{(2)}}{\partial l} = -\frac{1}{2\pi v_F}(\tilde{g}_2^{(1)}\tilde{g}_2^{(1)} - \tilde{g}_2^{(3)}\tilde{g}_2^{(3)}). \tag{20}$$

In the above equations, the variable l stands for minus the logarithm of the energy (temperature) scale measured in units of the high energy scale E_c of the 1D model (of the order of ∼0.1 eV).

In order to determine the electronic instabilities that may appear at low energies, we have solved the whole set of scaling equations, taking initial values for the couplings according to the above discussion. We take as free parameters the dielectric constant κ and the phonon-mediated e–e interaction with $q \approx 2k_F$, given by the pure number λ. λ spans between different estimates found in the literature.

The couplings approach in general a regime where they grow large as $l \to \infty$. Regarding the forward scattering interactions, $g_4^{(2)}$ becomes increasingly repulsive, leading to a singularity characterized by either the vanishing of K_+ or the divergence of K_-, depending on the region of the phase diagram. The scaling of the interactions stops at the low energy scale $\omega_c \equiv E_c e^{-l_c}$ corresponding to the point l_c where the singularity is reached. This has actually the character of a critical point, since it gives rise to the opening of a branch cut and nonanalytic behaviour in the corresponding Luttinger liquid parameter K_+ or K_- [14]. We have plotted in figure 2 the phase diagram of the (3, 3) nanotubes showing the two different regions of singular behaviour.

In general, the enhancement of backscattering and Umklapp interactions upon scaling may lead to a large growth of electron correlations, pointing at a tendency towards long range order in the electron system. We have analysed this possibility through the computation of different response functions

$$\chi(k,\omega) = -\mathrm{i}\int_{-\infty}^{+\infty} \mathrm{d}t \int_0^L \mathrm{d}x e^{\mathrm{i}\omega t} e^{\mathrm{i}kx} \langle T\, O(x,t) O(0,0)^\dagger \rangle \tag{21}$$

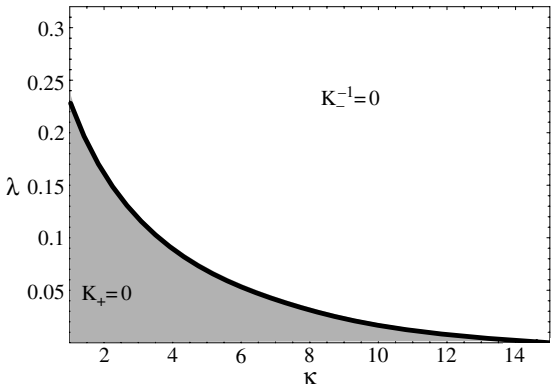

Figure 2. Phase diagram showing the different low energy instabilities in the array of (3, 3) nanotubes, depending on the dielectric constant κ and the effective coupling λ of the phonon-mediated interaction.

where the pair field O characterizes a particular type of ordering. In the system under consideration, the most important correlation functions are found to be given by the following (Fourier transformed) fields:

$$O_{\mathrm{DW},\mu}(k \approx 2k_{\mathrm{F}}) = \frac{1}{2\sqrt{L}} \sum_{p,\alpha,\beta} \left[\Psi^{\dagger}_{R1\alpha}(p-k)\sigma_{\mu}^{\alpha,\beta}\Psi_{L2\beta}(p) + \Psi^{\dagger}_{L1\alpha}(p-k)\sigma_{\mu}^{\alpha,\beta}\Psi_{R2\beta}(p) \right]$$

$$O_{\mathrm{DW}',\mu}(k \approx 0) = \frac{1}{2\sqrt{L}} \sum_{p,\alpha,\beta} \left[\Psi^{\dagger}_{R1\alpha}(p-k)\sigma_{\mu}^{\alpha,\beta}\Psi_{L1\beta}(p) + \Psi^{\dagger}_{R2\alpha}(p-k)\sigma_{\mu}^{\alpha,\beta}\Psi_{L2\beta}(p) \right],$$

$$O_{\mathrm{SC},\mu}(k \approx 0) = \frac{1}{2\sqrt{L}} \sum_{p,\alpha,\beta} \alpha \left[\Psi_{R1\alpha}(-p+k)\sigma_{\mu}^{-\alpha,\beta}\Psi_{L2\beta}(p) + \Psi_{R2\alpha}(-p+k)\sigma_{\mu}^{-\alpha,\beta}\Psi_{L1\beta}(p) \right],$$

where Ψ_{ris} represents the electron field with chirality $r = L, R$ (left, right moving character) at the Fermi point $i = 1, 2$ and spin projection s. For density wave (DW) operators, $\mu = 0$ corresponds to a charge density wave (CDW) and $\mu = 1, 2, 3$ to a spin density wave (SDW), while for superconducting (SC) operators, $\mu = 0$ stands for singlet superconductivity and $\mu = 1, 2, 3$ for triplet superconductivity ($\sigma_{\mu}^{\alpha,\beta}$ are the Pauli matrices, with $\sigma_{0}^{\alpha,\beta} = \mathbf{1}_{2\times 2}$).

The derivatives with respect to the frequency of the response functions obey actually scaling equations [3], whose solution allows one to compare the relative growths of the different electron correlations. By looking at the low energy scaling, we have checked however that none of the response functions shows a very large growth, down to the point where the scaling flow breaks down due to the singularity in the Luttinger liquid parameter. This singular behaviour occurs therefore before the appearance of any tendency to long range order in the electron system. This is illustrated for a typical instance in figure 3, where it can be observed that only the CDW correlations with vanishing momentum show a significant growth as the critical point is approached, while the superconducting correlations remain all small.

This finding seems to rule out the possibility of having superconducting correlations in the (3, 3) nanotubes, at least under the physical conditions considered in the present paper. We coincide in this respect with the conclusions reached in previous analyses by means of other computational methods [11, 15]. We have found however that the appearance of a CDW instability is precluded by the breakdown of the Luttinger liquid behaviour, which cuts off the

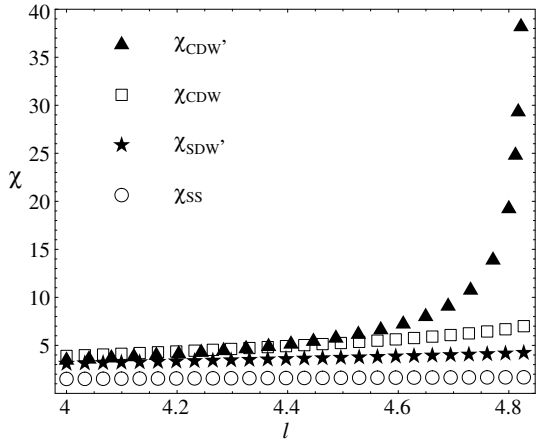

Figure 3. Plot of different response functions at $\kappa = 2$ and $\lambda = 0.1$.

growth of the different correlations. The destabilization of the Luttinger liquid is favoured in this respect by the screening effects from the 3D array of nanotubes, which are responsible for bringing the Coulomb interaction into the weak coupling regime.

3.2. (5, 0) nanotube

In the (5, 0) geometry, the most interesting scenario arises in the doped regime, when the Umklapp processes vanish because of momentum conservation [7]. In this case the scaling equations read

$$\frac{\partial g_1^{(1)}}{\partial l} = -\frac{1}{\pi v_F}(g_1^{(1)} g_1^{(1)} + g_1^{(2)} g_2^{(1)}) - \frac{1}{\pi v_F}\beta u_F u_B \tag{22}$$

$$\frac{\partial g_1^{(2)}}{\partial l} = \left(1 - \frac{1}{K_-}\right) g_1^{(2)} - \frac{1}{\pi v_F}(g_2^{(1)} g_1^{(1)} + (\beta/2)(u_F^2 + u_B^2)) \tag{23}$$

$$\frac{\partial g_2^{(1)}}{\partial l} = \left(1 - \frac{1}{K_-}\right) g_2^{(1)} - \frac{1}{\pi v_F}(2g_4^{(1)} g_2^{(1)} - g_4^{(1)} g_1^{(2)} + g_1^{(2)} g_1^{(1)} + \beta u_F u_B + 12\tilde{g}_4^{(1)} \tilde{g}_2^{(1)}) \tag{24}$$

$$\frac{\partial g_2^{(2)}}{\partial l} = -\frac{1}{2\pi v_F}(g_2^{(1)} g_2^{(1)} + g_1^{(1)} g_1^{(1)} + g_1^{(2)} g_1^{(2)}) \tag{25}$$

$$\frac{\partial g_4^{(1)}}{\partial l} = -\frac{1}{\pi v_F}(g_4^{(1)} g_4^{(1)} + g_2^{(1)} g_2^{(1)} - g_1^{(2)} g_2^{(1)} + 6\tilde{g}_4^{(1)} \tilde{g}_4^{(1)} + 6\tilde{g}_2^{(1)} \tilde{g}_2^{(1)}) \tag{26}$$

$$\frac{\partial g_4^{(2)}}{\partial l} = -\frac{1}{2\pi v_F}(g_4^{(1)} g_4^{(1)} - g_1^{(2)} g_1^{(2)}) \tag{27}$$

$$\frac{\partial g^{(2)}}{\partial l} = -\frac{1}{\pi v_F}((\beta/2) g^{(1)} g^{(1)} + u_F^2 + u_B^2) \tag{28}$$

$$\frac{\partial g^{(1)}}{\partial l} = -\frac{1}{\pi v_F}(\beta g^{(1)} g^{(1)} + 2u_F u_B) \tag{29}$$

$$\frac{\partial f^{(2)}}{\partial l} = -\frac{\alpha}{2\pi v_F}(f^{(1)} f^{(1)} - u_F^2) \tag{30}$$

$$\frac{\partial f^{(1)}}{\partial l} = -\frac{\alpha}{\pi v_{\mathrm{F}}}(f^{(1)} f^{(1)} + u_{\mathrm{B}}^2 - u_{\mathrm{F}} u_{\mathrm{B}}) \tag{31}$$

$$\frac{\partial u_{\mathrm{F}}}{\partial l} = \Delta u_{\mathrm{F}} - \frac{1}{2\pi v_{\mathrm{F}}}(g_1^{(2)} u_{\mathrm{F}} + (g_2^{(1)} + g_1^{(1)} + \beta g^{(1)}) u_{\mathrm{B}}) \tag{32}$$

$$\frac{\partial u_{\mathrm{B}}}{\partial l} = \Delta u_{\mathrm{B}} - \frac{1}{2\pi v_{\mathrm{F}}}(g_1^{(2)} u_{\mathrm{B}} + (g_2^{(1)} + g_1^{(1)} + \beta g^{(1)}) u_{\mathrm{F}}) + \frac{\alpha}{\pi v_{\mathrm{F}}} f^{(1)}(u_{\mathrm{F}} - 2u_{\mathrm{B}}) \tag{33}$$

$$\frac{\partial \tilde{g}_2^{(1)}}{\partial l} = -\frac{1}{\pi v_{\mathrm{F}}}(2g_4^{(1)}\tilde{g}_2^{(1)} + 2g_2^{(1)}\tilde{g}_4^{(1)} + 4\tilde{g}_4^{(1)}\tilde{g}_2^{(1)} + \tilde{g}_2^{(2)}\tilde{g}_2^{(1)} - g_4^{(2)}\tilde{g}_2^{(1)} - g_1^{(2)}\tilde{g}_4^{(1)}) \tag{34}$$

$$\frac{\partial \tilde{g}_4^{(1)}}{\partial l} = -\frac{1}{\pi v_{\mathrm{F}}}(2g_4^{(1)}\tilde{g}_4^{(1)} + 2g_2^{(1)}\tilde{g}_2^{(1)} + 2\tilde{g}_4^{(1)}\tilde{g}_4^{(1)} + 2\tilde{g}_2^{(1)}\tilde{g}_2^{(1)} + \tilde{g}_4^{(2)}\tilde{g}_4^{(1)} - g_4^{(2)}\tilde{g}_4^{(1)} - g_1^{(2)}\tilde{g}_2^{(1)}) \tag{35}$$

$$\frac{\partial \tilde{g}_4^{(2)}}{\partial l} = -\frac{1}{2\pi v_{\mathrm{F}}}\tilde{g}_4^{(1)}\tilde{g}_4^{(1)} \tag{36}$$

$$\frac{\partial \tilde{g}_2^{(2)}}{\partial l} = -\frac{1}{2\pi v_{\mathrm{F}}}\tilde{g}_2^{(1)}\tilde{g}_2^{(1)}, \tag{37}$$

where $\beta = v_{\mathrm{F}}/v_{\mathrm{F}}^{(0)}$, $\alpha = 2/(1 + v_{\mathrm{F}}^{(0)}/v_{\mathrm{F}})$ and the anomalous dimension Δ in equations (32) and (33) has been evaluated in detail in [8]. In this case the dielectric constant κ is the only free parameter, since the electron–phonon interaction was estimated with great accuracy in [10].

The dominant response functions are dictated by $O_{\mathrm{DW},\mu}(k \approx 2k_{\mathrm{F}})$ defined in the previous section and by the following bilinears:

$$O^{P}_{\mathrm{DW}''',\mu}(k \approx k_{\mathrm{F}_{L0}} - k_{\mathrm{F}_{R1}}) = \frac{1}{2\sqrt{L}}\sum_{p,\alpha,\beta}\Big[\Psi^{\dagger}_{R1\alpha}(p-k)\sigma_{\mu}^{\alpha,\beta}\Psi_{L0\beta}(p) + P\ \Psi^{\dagger}_{R0\alpha}(p-k)\sigma_{\mu}^{\alpha,\beta}\Psi_{L2\beta}(p)\Big],$$

$$O^{P,Q}_{\mathrm{SC},\mu}(k \approx 0) = \frac{1}{\sqrt{3L}}\sum_{p,\alpha,\beta}\big[\Psi_{R1\alpha}(-p+k)\sigma_{\mu}^{\alpha,\beta}\Psi_{L2\beta}(p) + P\Psi_{R2\alpha}(-p+k)\sigma_{\mu}^{\alpha,\beta}\Psi_{L1\beta}(p) + Q\Psi_{R0\alpha}(p-k)\sigma_{\mu}^{\alpha,\beta}\Psi_{L0\beta}(p)\big],$$

where $P, Q = \pm 1$ take into account the band entanglement [12].

We have plotted in figure 4 a typical flow of the dominant response functions up to the energy scale at which the divergence of the charge stiffness occurs. We note that the tendency to CDW ordering characterizing the (3, 3) geometry is replaced by an enhancement of the superconducting correlations, which is the most remarkable feature of this system. Anyway, the values of $\chi_{SS}^{1,1}$ do not grow large, making it unlikely that they give rise to an observable feature. Indeed the physical regime is of the same kind of that of the (3, 3) case. The instability of the system is not characterized by the development of any kind of (quasi-)long range order, but by the divergence of the charge stiffness.

We point out that the above results cannot be likened to those obtained within the usual two-band model of metallic nanotubes. The main difference is the development of superconducting correlations in the present model, which are completely absent, for instance, in the (3, 3) geometry [16]. This is due to the influence of new couplings, like u_{F} and u_{B}, which enhance $\chi_{SS}^{1,1}$ when driven to the attractive regime. We also note that the divergence of the charge susceptibility provides a regime of phase separation into regions with different electronic densities, referred to a sector of the model in which the three low energy subbands are entangled through the coupling $f^{(2)}$, which is a peculiar feature of the three-band model.

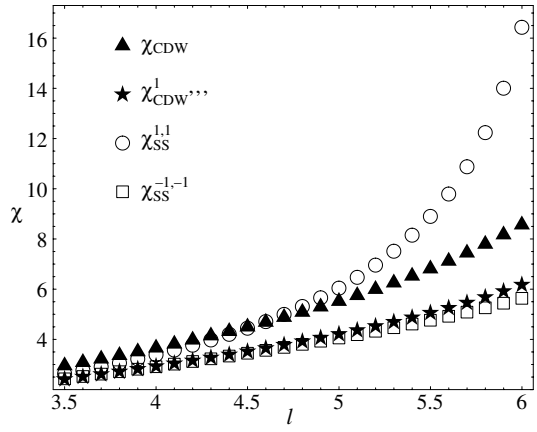

Figure 4. Flow of the largest response functions at $\kappa = 2$.

4. Discussion and conclusions

The (3, 3) carbon nanotubes may fall into two different low temperature phases, whose physical properties are dictated by the vanishing of K_+ and the divergence of K_- respectively. We recall in particular that, for the experimental set-up of reference [2], a reasonable choice of the parameters is $\kappa \sim 2$–4 and $\lambda \sim 0.1$, corresponding to the $K_+ = 0$ phase. In this case the temperature of transition to the new phase turns out to be strongly dependent on the dielectric constant of the environment, ranging from $T_c \sim 10^{-1}$ K (at $\kappa \approx 2$) to $T_c \sim 10$ K (at $\kappa \approx 4$).

We have shown that, even considering the large screening effects from the arrays of nanotubes in the experimental samples, the effective e–e attraction arising from the exchange of phonons is not large enough to support the appearance of superconducting correlations in the (3, 3) nanotubes. The experimental conditions of the samples described in [2] seem to place the system in the region of the phase diagram characterized by the vanishing of K_+. This leads to the vanishing of the conductivity at the point of the transition, as follows from equation (5). Moreover, it also gives rise to the vanishing of the tunnelling conductance, which is directly related to the tunnelling density of states $n(\varepsilon)$. Within the Luttinger liquid framework, the latter follows the low energy behaviour

$$n(\varepsilon) \sim \varepsilon^{(K_+ + 1/K_+ + K_- + 1/K_- - 4)/8}. \tag{38}$$

The depletion of the density of states given by equation (38) at vanishing K_+ is consistent with the appearance of the pseudogap observed experimentally in the measures of the I–V characteristics reported in [2]. The critical point characterized by the vanishing of K_+ does not describe however a conventional metal–insulator transition, as long as the compressibility given by equation (4) remains finite at the point of the transition. As analysed in [16], the critical point implies actually a divergent diamagnetic susceptibility, as a consequence of the development of very soft modes in the sector of electron current excitations. Therefore, the phenomenology derived from the $K_+ = 0$ phase of the (3, 3) carbon nanotubes seems to be consistent, at least qualitatively, with the main experimental signatures reported in [2].

In the (5, 0) geometry the scenario is different. Superconducting correlations develop due to the strong electron–phonon coupling. Before they may grow large, a singularity is reached in one of the Luttinger liquid parameters. The divergence of the charge stiffness signals the onset of a regime of strong attraction, as it implies the divergence of the compressibility and density–density correlator in the corresponding sector and the vanishing of the renormalized Fermi

velocity as well. This points to the development of phase separation into spatial regions with different electronic densities, in close analogy with the physical interpretation of the Wentzel–Bardeen singularity. For the zeolite matrix of reference [2], the estimate of the dielectric constant gives $\kappa \approx 2$–4, which corresponds to a transition temperature $T_c \approx 3$–20 K.

Finally, we end up with a picture consistent with the experimental observations reported in [2] assuming that, as supported by the measurements of the nanotube diameter, most of the CN contained in the zeolite matrix have preferentially a (3, 3) geometry. Further experimental work would be needed to clarify the existence of such a critical point in the (3, 3) nanotubes, its physical properties and its stability under changes of relevant experimental conditions.

Acknowledgments

The financial support of the Ministerio de Educación y Ciencia (Spain) through grant BFM2003-05317 is gratefully acknowledged. EP was also supported by INFN grant 10068.

References

[1] Tang Z K, Sun H D, Wang J N, Chen J and Li G D 1997 *Appl. Phys. Lett.* **73** 2287
[2] Tang Z K, Zhang L, Wang N, Zhang X X, Wen G H, Li G D, Wang J N, Chan C T and Sheng P 2001 *Science* **292** 2462
[3] Sólyom J 1979 *Adv. Phys.* **28** 201
[4] Krotov Yu A, Lee D-H and Louie S G 1997 *Phys. Rev. Lett.* **78** 4245
[5] Liu H J and Chan C T 2002 *Phys. Rev.* B **66** 115416
[6] Cabria I, Mintmire J W and White C T 2003 *Phys. Rev.* B **67** R121406
[7] Egger R and Gogolin A O 1997 *Phys. Rev. Lett.* **79** 5082
Egger R and Gogolin A O 1998 *Eur. Phys. J.* B **3** 281
[8] González J and Perfetto E 2005 *Phys. Rev.* B **72** 205406
Gozalez J and Perfetto E 2005 *Preprint* cond-mat/0510586
[9] Hawrylak P, Eliasson G and Quinn J J 1988 *Phys. Rev.* B **37** 10187
[10] Barnett R, Demler E and Kaxiras E 2005 *Phys. Rev.* B **71** 035429
[11] Connétable D, Rignanese G-M, Charlier J-C and Blase X 2005 *Phys. Rev. Lett.* **94** 015503
[12] Sédéki A, Caron L G and Bourbonnais C 2002 *Phys. Rev.* B **65** R140515
[13] Schulz H J 1993 *Correlated Electron Systems* vol 9, ed V J Emery (Singapore: World Scientific)
[14] Alvarez J V and González J 2003 *Phys. Rev. Lett.* **91** 076401
[15] Bohnen K-P, Heid R, Liu H J and Chan C T 2004 *Phys. Rev. Lett.* **93** 245501
[16] González J 2005 *Phys. Rev.* B **72** 73403